Journal of Crystal Growth 311 (2009) 4619–4627

Contents lists available at ScienceDirect

Journal of Crystal Growth

journal homepage: www.elsevier.com/locate/jcrysgro

Synchrotron topography and X-ray diffraction study of GaInP layers grown on GaAs/Ge

A. Lankinen [a,*], L. Knuuttila [a,b], P. Kostamo [a], T.O. Tuomi [a], H. Lipsanen [a], P.J. McNally [c], L. O'Reilly [c]

[a] Department of Micro and Nanosciences, Helsinki University of Technology, P.O. Box 3500, FIN-02015 TKK, Finland
[b] OptoGaN GmbH, Konrad-Adenauer-Allee 11, 44263 Dortmund, Germany
[c] Research Institute for Networks and Communications Engineering, Dublin City University, Dublin 9, Ireland

ARTICLE INFO

Article history:
Received 23 February 2008
Received in revised form
29 August 2009
Accepted 31 August 2009
Communicated by M.S. Goorsky
Available online 8 September 2009

PACS:
61.72.Ff
61.72.Lk
61.72.Mm
65.40.De
81.05.Ea
81.15.Gh

Keywords:
A1. X-ray topography
A1. X-ray diffraction
A1. Interfaces
A1. Crystallites
A3. Metalorganic vapor phase epitaxy
B2. Semiconducting indium gallium phosphide

ABSTRACT

$Ga_{1-x}In_xP$ layers are grown on GaAs/Ge substrates by metalorganic vapor phase epitaxy and studied by means of synchrotron X-ray topography and high-resolution X-ray diffractometry. Misfit dislocations (MDs) in $Ga_{0.5094}In_{0.4906}P$ epilayers having a $+3.8\times10^{-4}$ lattice mismatch to GaAs/Ge substrates at room temperature (RT) are observed. $Ga_{0.4995}In_{0.5005}P$ epilayers having a lattice mismatch of -3.5×10^{-4} to the GaAs/Ge substrates at RT are shown to be free of MDs, which is explained by the different linear thermal expansion coefficient of the epilayer from that of the substrate material compensating the lattice mismatch at the growth temperature of 610 °C. The Matthews–Blakeslee model for critical thickness was matched to the observed MD pattern in the samples. Additionally, faceted InP hillocks and strain fields beneath them are observed within the GaInP layers. The observed MDs, which are most likely of the 60° mixed $\langle 1\,0\,1\rangle\{1\,1\,1\}$ type, originate at the hillocks.

1. Introduction

The highest performance solar cells nowadays are multi-junction devices based on Ge, GaAs and GaInP. The devices are made by depositing thin films of GaAs and GaInP on Ge substrates, and they have been widely used in space applications due to their high efficiency [1]. However, when heteroepitaxial techniques are applied to single crystal semiconductor manufacturing processes, additional difficulties related to lattice mismatch and thermal expansion may occur.

In this work, crystal properties of GaInP layers grown by metalorganic vapor phase epitaxy (MOVPE) on GaAs/Ge substrates are studied. GaAs/Ge substrates consist of 200–250 nm thick high-quality GaAs buffer layers grown by MOVPE on commercial practically dislocation-free Ge substrates. The GaAs/Ge structures used as substrates in this work are of a high crystal quality and have been previously studied in [2,3]. The main idea for using the GaAs/Ge substrates is to apply prior knowledge about growing GaInP on GaAs [4–7] to Ge substrates with only minor modifications. Also, problems with anti-phase domains (APD) appearing in GaAs epilayers on Ge were already solved in a previous publication [2], and by using GaAs/Ge substrates instead of plain Ge substrate the possible problem of APD formation on GaInP/Ge interface is probably avoided.

Synchrotron radiation X-ray topography (SR-XRT) [8] and high-resolution X-ray diffractometry (HR-XRD) measurements are non-destructive methods for studying high quality crystalline materials with X-rays. SR-XRT is used to obtain data on the spatial distribution and type of the crystal defects, and on the strain fields inside the samples. In this study specific attention is paid to diffraction imaging of misfit dislocations (MD) with SR-XRT. HR-XRD is best suited for acquiring accurate lattice constant and

* Corresponding author. Tel.: +358 94513120; fax: +358 94513128.
E-mail addresses: aapo.lankinen@iki.fi, aapo.lankinen@tkk.fi (A. Lankinen).

0022-0248/$ - see front matter © 2009 Elsevier B.V. All rights reserved.
doi:10.1016/j.jcrysgro.2009.08.032

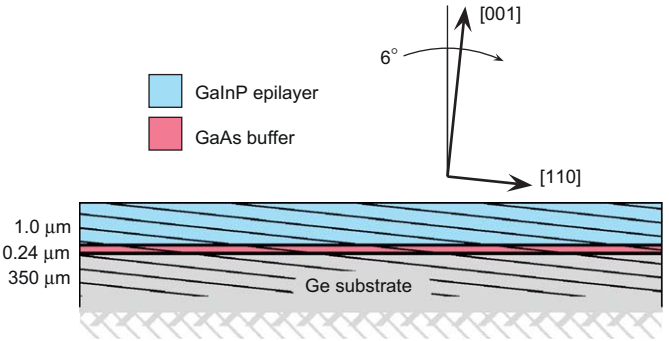

Fig. 1. Schematic drawing of the cross-section of a GaInP/GaAs/Ge sample. The (0 0 1) Ge substrate lattice is 6° off-oriented towards ⟨1 1 1⟩.

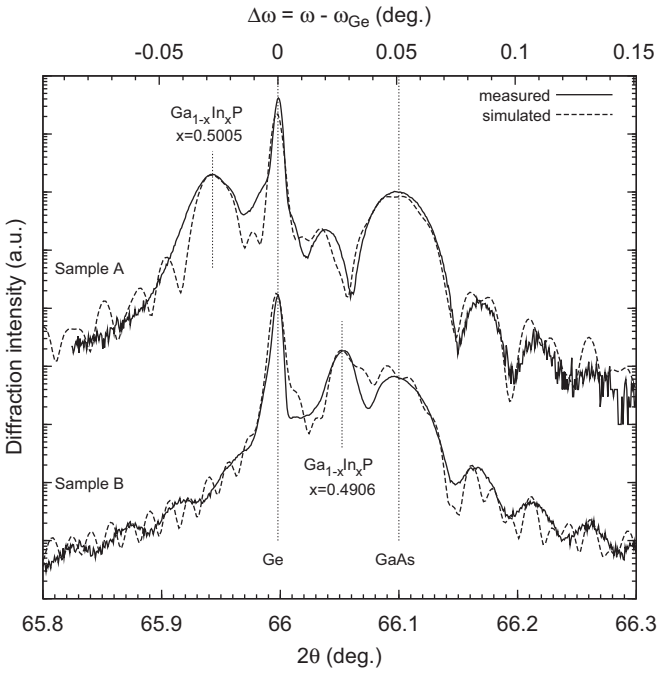

Fig. 2. $2\theta/\omega$ 004 HR-XRD curves and corresponding simulations of samples A and B. $\Delta\omega = \omega - \omega_{Ge}$, in which ω is the angle between the sample surface and the incident X-ray beam, and ω_{Ge} is the Ge substrate peak position.

lattice orientation data of macroscopic volumes of the sample. The GaInP epilayers were studied with both of these methods in order to reveal MDs and other crystal defects in the epilayers.

2. Experimental

The GaAs and The GaInP epitaxial layers were grown by Thomas Swan low-pressure vertical close-coupled showerhead reactor. The GaInP epilayers were deposited on the 0.24 μm thick GaAs buffer, which was grown on (0 0 1) Ge substrate 6° off-oriented towards ⟨1 1 1⟩. For the group V atoms tertiarybutyls and for the group III atoms trimethyls were used as precursors. The growth pressure was 100 Torr. The GaAs buffer layers were deposited using a relatively low growth temperature of 550 °C and a V/III ratio of 7.5. The growth of GaInP layers was performed at 610 °C with a V/III ratio of about 60.

The two samples under study have different indium contents, which was achieved by changing trimethylindium (TMIn) flow between the MOVPE growth runs. Specifically, the TMIn flow was 2.1% smaller for sample B than for sample A, while trimethylgallium (TMGa) flow was kept constant, resulting in lower In content in sample B. The In content x in the $Ga_{1-x}In_xP$ layer of both samples was chosen to be close to a compound that is lattice matched to Ge. Fig. 1 shows a cross-sectional schematic drawing of the layer structure for both samples. Zeiss Supra 40 scanning electron microscope (SEM) and Leitz Laborlux 12 HL optical microscope were used for acquiring images of surface features on the samples.

HR-XRD curves of the GaInP samples were measured using Philips X'Pert PRO diffractometer in triple axis configuration. The triple axis mode has a Ge-220 three-crystal analyzer in front of the detector, which allows accurate determination of both the angle between the incident beam and the sample surface ω, and the diffraction angle 2θ. The divergence $\delta\omega$ of the incident beam is reduced by the Ge-220 four-crystal monochromator positioned in the beam emitted by the Cu anode X-ray tube ($\delta\omega \approx 12$ arcsec). Standard resolution X-ray diffraction (XRD) geometry without the monochromator and analyzer having lower accuracy but higher sensitivity was used for analyzing small crystallites. The measured XRD and HR-XRD curves are plotted as a function of 2θ. Because ω is also changed so that the sample remains in the Bragg condition, the curves are called $2\theta/\omega$ XRD and HR-XRD curves.

SR-XRT was performed at the topography station F1 of the Hamburger Synchrotronstrahlungslabor (HASYLAB) at the Deutsches Elektronen-Synchrotron (DESY) in Hamburg using the continuous spectrum of radiation emitted by a bending magnet source on the DORIS storage ring. For a review of synchrotron X-ray topography of electronic materials see [9]. The positron momentum was 4.436 GeV/c and the current ranged from 94 mA to 143 mA. Several high-resolution topographs were recorded on high-resolution GEOLA VRP-M films set 60 mm in front of or behind the sample in the back-reflection and the transmission geometry, respectively. For the section topography the beam was narrowed by a horizontal slit having a width of ≈15 μm. A typical exposure was 300 mA · min in the large-area mode and 3000 mA · min in the section mode. The sample surface was set perpendicularly to the incident beam in the large-area transmission geometry. In the large-area back-reflection and in the section transmission geometries the sample was additionally rotated 6° and 16° around the horizontal axis perpendicular to the incident beam, in order to ascertain the appearance of small-index reflections, such as 004 and 220, on the X-ray film.

3. Results and discussion

Fig. 2 shows 004 HR-XRD curves of samples A and B and the corresponding simulations. Based on the simulations one would expect to see XRD fringes caused by interference between Ge, GaAs and $Ga_{1-x}In_xP$ peaks. However, the small and narrow fringes related to $Ga_{1-x}In_xP$ do not exist in the measured curves of Fig. 2, and only the large and wide fringes related to GaAs and Ge are visible. This is likely caused by imperfections in the $Ga_{1-x}In_xP$ layers, which is also suggested by the broadening of the measured $Ga_{1-x}In_xP$ layer peaks compared to the simulated ones. The lattice parameters and other data extracted from the simulations are listed in Table 1. $Ga_{1-x}In_xP$ lattice mismatches to Ge substrate $f = \Delta a/a$ at growth temperature are calculated using lattice constants at growth temperature a_{GT} derived from linear thermal expansion coefficients α_{ltc} by $a_{GT} = (1+\alpha_{ltc}\Delta T)a_{RT}$, where a_{RT} is the room temperature (RT) lattice constant and ΔT is the difference between RT and the growth temperature.

Fig. 3(a) shows a 224 reciprocal space map (RSM) of sample A, i.e. the diffracted X-ray intensity contours as a function of the reciprocal space axes q_z and q_{xy}. Using an asymmetrical

Table 1
Properties of samples A and B.

	Sample A	Sample B
GaAs buffer thickness (μm)	0.23	0.24
$Ga_{1-x}In_xP$ thickness (μm)	1.0	1.0
$Ga_{1-x}In_xP$ In content x	0.5005	0.4906
$f=\Delta a/a_0$ for $Ga_{1-x}In_xP$		
at RT	-3.5×10^{-4}	$+3.8\times10^{-4}$
at 610 °C	$+3.6\times10^{-4}$	$+10.9\times10^{-4}$
$Ga_{1-x}In_xP$ molar flows		
TMGa (μmol/min)	23.55	23.55
TMIn (μmol/min)	21.63	21.18

$Ga_{1-x}In_xP$ lattice mismatches to Ge $f=\Delta a/a=(a_{Ge}-a_0)/a_0$ (a_0 is the stress-free bulk lattice parameter of the $Ga_{1-x}In_xP$ epilayer) at room temperature (RT) are calculated from the lattice spacings d_{004} extracted from Fig. 2 assuming zero relaxation, whereas at 610 °C they have been extrapolated using RT linear thermal expansion coefficients α_{ltc} from [10,11] and lattice constants from [12–14].

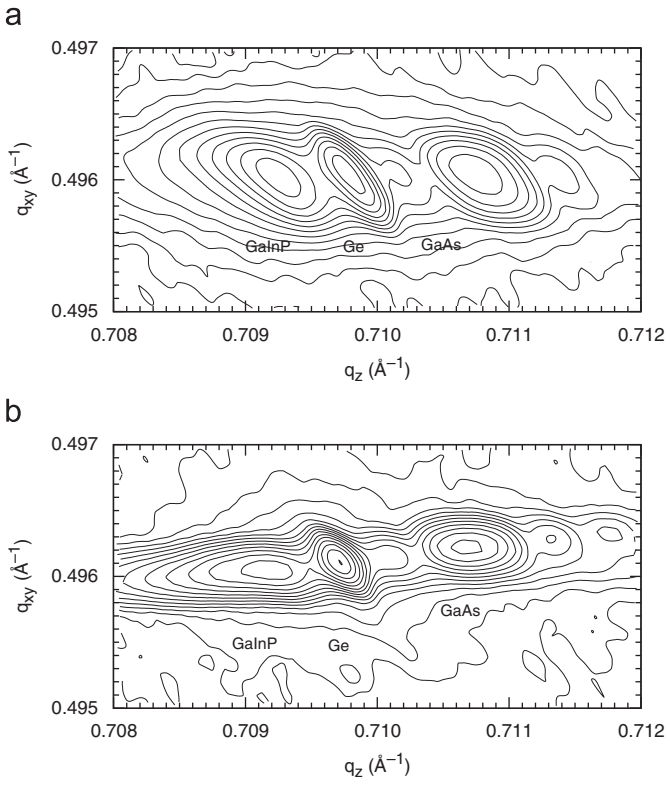

Fig. 3. HR-XRD 224 reciprocal space map of sample A measured: (a) in an orientation where the miscut angle is perpendicular to the plane of the diffraction and (b) in an orientation where the miscut angle resides in the plane of the diffraction. Reciprocal lattice axes q_{xy} and q_z coincide with ⟨1 1 0⟩ and [0 0 1] crystal directions, respectively. Intensity doubles between adjacent contours.

diffraction, like the 224 diffraction here, it is possible to simultaneously measure the lattice plane spacings both in the growth axis [0 0 1] (coincides with q_z-axis) and in the sample surface directions ⟨1 1 0⟩ (coincides with q_{xy}-axis). The Ge, GaAs and GaInP diffraction peaks in sample A are observed to lie on a horizontal line in the RSM of Fig. 3(a), which indicates that the sample layers are parallel and have equal interplanar spacings $d_{\{2\,2\,0\}}\approx 2.02\,A$. Thus, there is no relaxation observed within the measurement accuracy, which is limited by the sampling step of 0.005° in both 2θ and ω axes resulting in relative accuracies of $\Delta q_{xy}/q_{xy}\approx 1.3\times10^{-5}$ and $\Delta q_z/q_z\approx 8.0\times10^{-5}$. Similarly, the RSM of Fig. 3(a) shows that there is strain in the GaAs and the $Ga_{0.4995}In_{0.5005}P$ layers of sample A, which is evident from the lattice constant differences on the q_z-axis, i.e. growth direction [0 0 1].

The 224 RSM of Fig. 3(b) is measured so that the miscut angle of the substrate of sample A resides in the plane of the diffraction. The three diffraction peaks produced by the three layers are not lying on a horizontal line in the RSM, which is explained by additional tilt components between the lattices of the Ge substrate and of the GaAs and $Ga_{0.4995}In_{0.5005}P$ layers. It is a well-known fact that an additional tilt angle occurs between layer lattices along the miscut direction when III–V heteroepitaxy is performed on miscut substrates [15]. Comparing Figs. 3(a) and (b) it is observed that the same result holds for the GaInP grown on GaAs/Ge substrates.

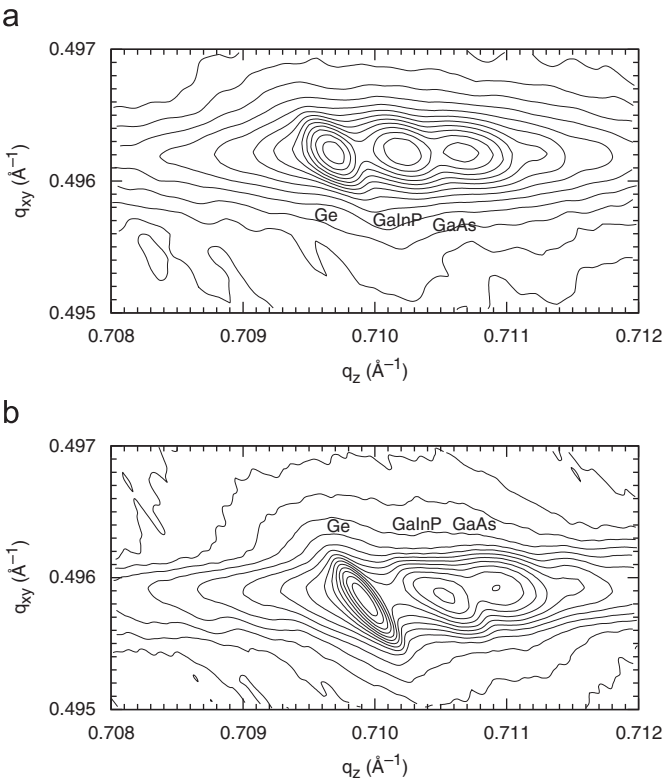

Fig. 4. HR-XRD 224 reciprocal space map of sample B measured: (a) in an orientation where the miscut angle is perpendicular to the plane of the diffraction and (b) in an orientation where the miscut angle resides in the plane of the diffraction. Reciprocal lattice axes q_{xy} and q_z coincide with ⟨1 1 0⟩ and [0 0 1] crystal directions, respectively. Intensity doubles between adjacent contours.

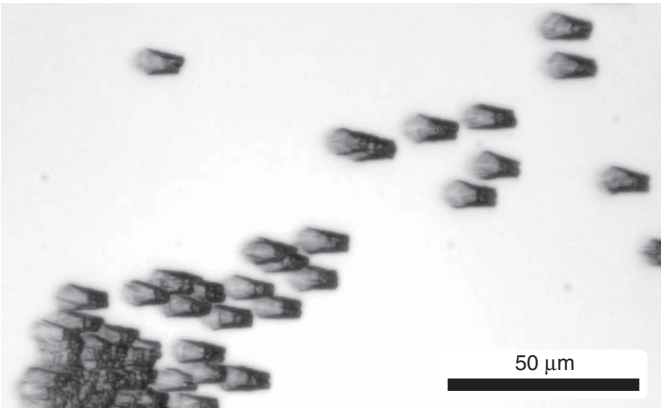

Fig. 5. Optical micrograph of sample A showing faceted hillocks on the surface.

The 224 RSM of sample B in Fig. 4(a) also has the Ge, GaAs and GaInP diffraction peaks on a horizontal line. Thus, there is very little or no relaxation present in the GaAs and GaInP layers of sample B, and the GaAs and $Ga_{0.5094}In_{0.4906}P$ layers are also strained in sample B. The strain is tensile in both epilayers of sample B, but the $Ga_{0.5094}In_{0.4906}P$ layer is less strained than the GaAs layer. 224 RSMs measured from $Ga_{1-x}In_xP$ epilayers having either large tensile strain ($x=0.41$) or large compressive strain ($x=0.55$) on GaAs substrates are known to show asymmetricity due to the asymmetric strain relaxation of $Ga_{1-x}In_xP$ on GaAs [16]. Some differences in the shapes of the X-ray maxima arising from the asymmetric strain is observed in RSMs of Figs. 3 and 4, but due to the relatively small strain in samples A and B, the differences in peak shapes between Figs. 3(a) and (b), or between Figs. 4(a) and (b), are minor.

Fig. 5 shows an optical micrograph of sample A. The features in the micrograph are large epitaxial hillocks on the GaInP layers.

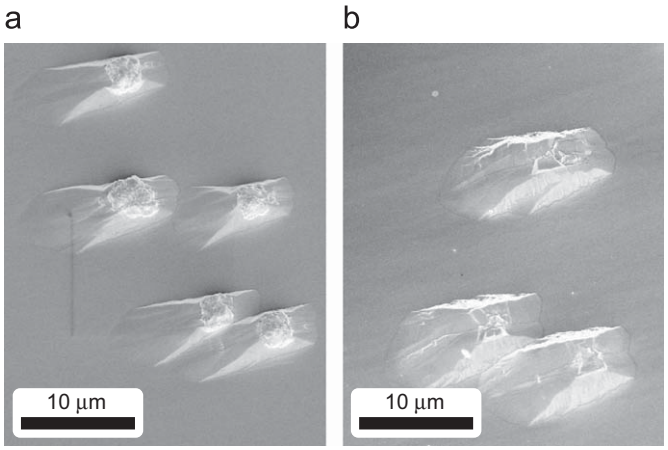

Fig. 6. Scanning electron micrographs of faceted hillocks: (a) on sample A and (b) on sample B. The electron beam energy was 5 keV.

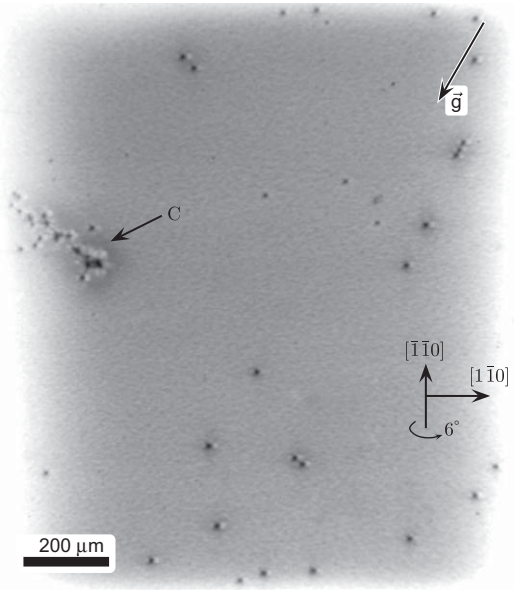

Fig. 7. 004 large-area back-reflection topograph of the GaInP sample A and the related diffraction vector *g*. The black dots are hillocks on the epitaxial layer. A cluster of hillocks is marked with C. The (0 0 1) Ge substrate has its 6° miscut angle towards [1 1̄ 1].

SEM pictures of the hillocks on samples A and B are shown in Fig. 6. The optical and SEM micrographs clearly show that the hillocks are faceted and have all the same size of $\approx 6\times 12\,\mu m^2$. Similar hillocks in $Ga_{1-x}In_xP/GaAs$ with $0.388\le x\le 0.552$ have been reported in [6], and they are a well-known problem in GaInP epitaxy [4,5,7]. However, it is possible to grow hillock-free GaInP layers using PH_3 as P precursor, if the PH_3 flow is modulated during the MOVPE growth [17].

Fig. 7 shows a large-area back-reflection topograph of sample A. The most distinct feature in the topograph is an assembly of dots, each displaying the same black–white contrast on the film. The dots are images of strain fields produced by the large epitaxial hillocks, the density of which was measured from Fig. 7 to be $\sigma_h\approx 1600-2600\,cm^{-2}$, depending on whether or not the hillocks in the cluster marked with C on the topograph are included in the value.

There are no MDs in sample A, which further proves that no relaxation has occurred during the growth process of sample A. Also, a careful inspection of the topograph of Fig. 7 reveals a pattern resembling an orange peel, which indicates that despite the absence of a MD network in the sample the crystal quality of the GaInP epilayer is not perfect. Such contrast variations in the diffraction image of the GaInP layer may originate from unhomogenous distribution of thermal strain, but this is uncertain. The lateral dimension of the features in the contrast pattern is $\approx 20\,\mu m$.

The observation that MDs are absent in sample A, even though the compressively strained GaInP epilayer has a lattice mismatch of $f=-3.5\times 10^{-4}$ between the relatively thick $Ga_{0.4995}In_{0.5005}P$ epilayer and the Ge substrate at RT (see Table 1), can be explained by the fact that the mismatch between the GaInP layer of sample A and the Ge substrate has about an equal magnitude but opposite sign at the growth temperature, $f=+3.6\times 10^{-4}$, as the $Ga_{0.4995}In_{0.5005}P$ epilayer strain turns to tensile due to the thermal expansion. Thus, the maximum of the magnitude of strain during the sample cooling from the growth temperature to RT is minimized in sample A. Similar results for MD-free epilayer growth have been demonstrated in the GaInP on GaAs material system when the GaInP is lattice matched to GaAs at the growth temperature [6]. It appears that the MDs are easily formed during the growth process itself at high temperature, rather than when cooling the sample back to RT.

Figs. 8(a)–(c) show large-area transmission topographs of sample A. The strain fields produced by the hillocks in the GaInP layer are clearly visible in the topographs. In Figs. 8(a) and (b) the black–white contrast of the strain field images follows the direction of the diffraction vector *g* so that the lighter contrast is on the positive side of *g*, which according to the eikonal approximation of the dynamical theory of diffraction indicates that the hillocks put the lattice beneath them under tensile strain [18]. However, the shape of the contrast produced by the hillock strain field is more complicated, as can be seen in the enlargement of the 331 topograph in Fig. 8(c). Inside the white half-arc the contrast is completely black, which can be interpreted as the strain of the lattice suddenly changing from compressive to tensile when going away from the center of the strain field [18]. Moreover, in the center of the hillock strain field image in Fig. 8(c) there is a small gray dot having a similar contrast to that produced by the defect-free GaInP lattice between hillocks, which by again applying the dynamical theory of diffraction [18] suggests that the strain directly under the center of the hillock is smaller than under its edges. Thus, the strain field inflicted to the surrounding GaInP/GaAs/Ge lattice by the hillock is rather complicated, being weak directly under the hillock, growing compressive under the edges of the hillock, but changing to tensile further away from the center.

The enlargement of the 331 topograph in Fig. 8(c) also demonstrates the similarity between the strain fields under three hillocks. The similarity of the size and the produced strain field of the hillocks suggests that they are remarkably homogenous and thus most likely produced by a decisive, yet unknown process. The center dot areas of the hillock strain fields in Fig. 8(c) may be related to the polycrystalline hillock core identified by Matragrano et al. in hillocks on GaInP layers using cross-sectional transmission electron microscopy [5].

Figs. 9(a) and (b) show transmission section topographs of sample A. Due to overexposure the image of the Ge substrate in the $\overline{1}\,\overline{3}\,1$ transmission topograph of Fig. 9(a) appears as a thick, featureless black horizontal line. The image of the GaInP epilayer is visible as a thinner dark gray line below it. The 220 transmission topograph of Fig. 9(b) has lower contrast showing details of strain fields in the Ge substrate, but no image of the GaInP epilayer is visible. The 230 nm thick GaAs buffer was too thin to produce any contrast at all in either topograph.

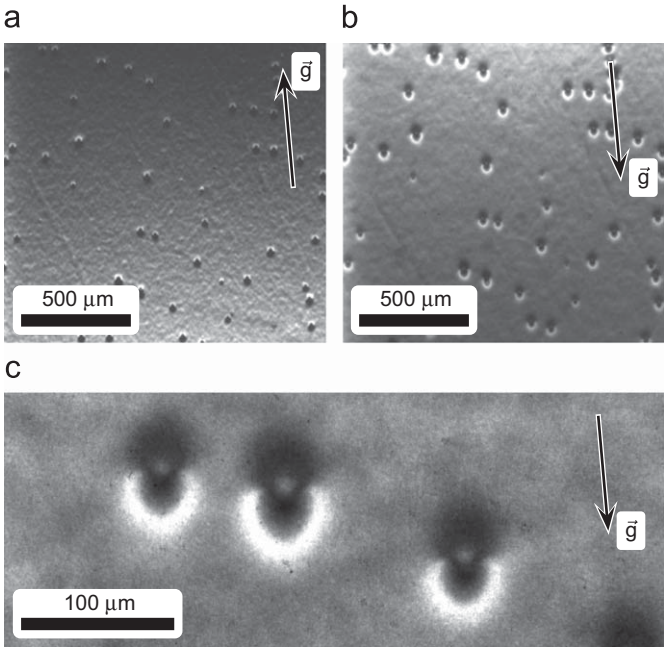

Fig. 8. (a) $\overline{2}\,\overline{2}\,0$, (b) 331 and (c) enlargement of 331 large-area transmission topographs of the GaInP sample A. The diffraction vector **g** projections are indicated.

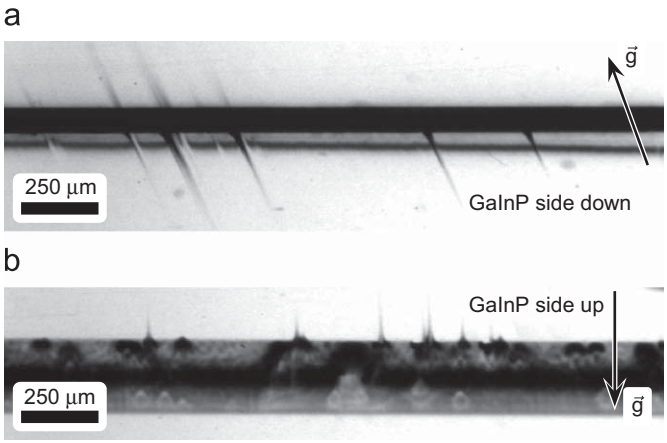

Fig. 9. (a) $\overline{1}\,\overline{3}\,1$ and (b) 220 transmission section topographs of the GaInP sample A and the related diffraction vector *g* projections. The epitaxial surface side in the section topographs is on the negative side of the *g*.

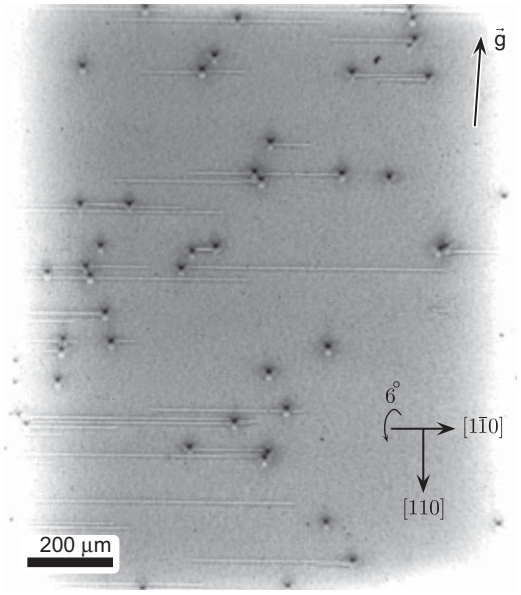

Fig. 10. 004 large-area back-reflection topograph of the GaInP sample B and the related diffraction vector *g*. The black-white dots are hillocks, whereas the white horizontal lines are misfit dislocations along [$\bar{1}$ 1 0] direction. The (0 0 1) Ge substrate has its 6° miscut angle towards [1 1 1].

The hillocks on the GaInP layer are observed to produce large strain fields, which have caused sharp streaks following diffraction vector *g* projections in the topographs of Figs. 9(a) and (b). Also, the hillock positions in GaInP lattice produce no contrast, thus appearing as white breaks in the GaInP epilayer line in Fig. 9(a). The GaInP/GaAs/Ge structure exhibits considerable thermal and lattice mismatch strain, which is visible in the topograph of Fig. 9(a) as a slight curvature of the epilayer line caused by rotation of the strained $(\overline{1}\,\overline{3}\,1)$ lattice planes of $Ga_{1-x}In_xP$.

The 004 large-area back-reflection topograph of sample B in Fig. 10 is otherwise similar to the topograph of sample A in Fig. 7, but there are horizontal white lines visible in the topograph of sample B. The white lines in Fig. 10 are images of MDs either in the interface between GaInP and GaAs or in the interface between GaAs and Ge. Most of the MDs are observed to either have their endpoints in the hillocks, or to go through the hillocks. This phenomenon can be explained by the increased strain inflicted into the GaInP lattice by the hillocks causing MD formation. The idea that the hillocks may act as sources for MD formation was first suggested by Matragrano et al. based on cathodoluminescence observations in [5]. Their hypothesis is strongly supported by the relation between the MDs and the hillocks observed in Fig. 10. Because most of the MDs either go through or end at the hillocks in the GaInP layer, it is also reasonable to assume that the MDs indeed reside in the interface between GaInP and GaAs. This would be further suggested by the fact that a 240-nm-thick GaAs layer, as used for the buffer layer, could be grown about three times as thick without MDs appearing in GaAs/Ge interface [3].

Sample B has MD density of $\sigma_{MD} \approx 1700\,cm^{-2}$, which was estimated from the topograph of Fig. 10. The existence of MDs in Fig. 10 can be explained by considering that even though the $Ga_{0.5094}In_{0.4906}P$ epilayer in sample B is almost lattice matched to Ge at RT, there is a lattice mismatch of about $f = +10.9 \times 10^{-4}$ at the growth temperature. This further highlights the importance of lattice matching at growth temperature in heteroepitaxy. The

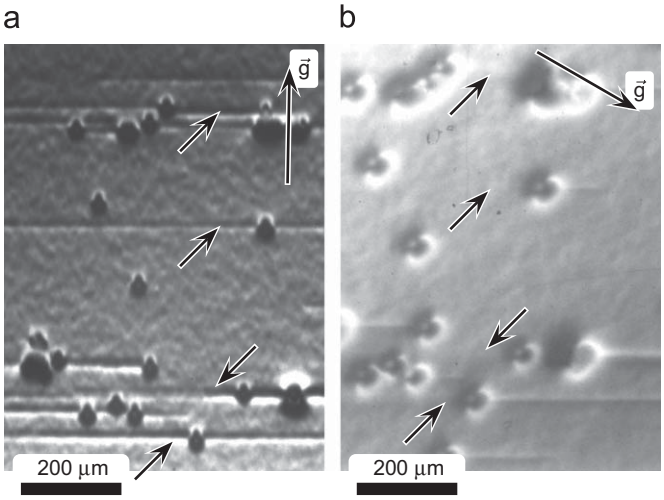

Fig. 11. (a) $\overline{2}\,\overline{2}\,0$ and (b) $\overline{1}\,5\,1$ large-area transmission topographs of the GaInP sample B and the related diffraction vector $\boldsymbol{g}$ projections. The arrows indicate the positions of disappearing misfit dislocation lines in (a), and corresponding locations in (b) where their images have disappeared.

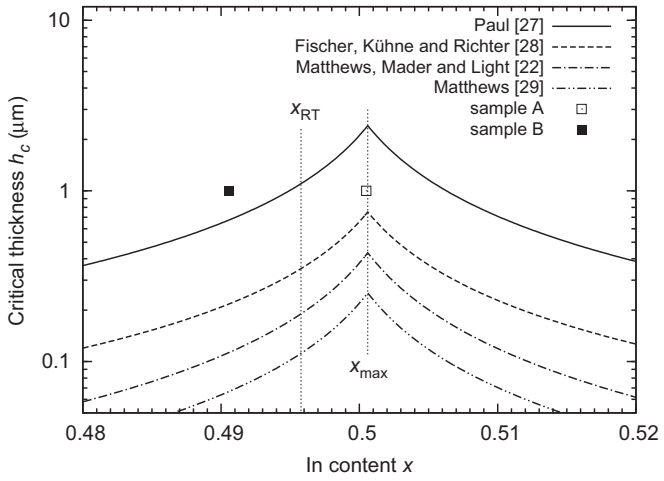

Fig. 12. Critical thicknesses of $Ga_{1-x}In_xP$ on Ge plotted as a function of In content x calculated from the theoretical models suggested by Paul [27], Fischer et al. [28], Matthews et al. [22], and Matthews (assuming relaxation through pure edge dislocations) [29]. The curves take into account the maximum strain occuring when cooling down from 610 °C to room temperature (RT). Vertical dotted lines indicate In contents x_{RT} of $Ga_{1-x}In_xP$ lattice matched to Ge at RT and x_{max} of the maximum attainable critical thickness within the temperature range. Thicknesses and In contents of samples A and B are also indicated onto the graph. Note that only sample B actually contains misfit dislocations.

dislocation lines in Fig. 10 are observed to run parallel to the $[1\,\overline{1}\,0]$ axis, around which the 6° off-orientation is tilted. Remarkably, the MDs are completely absent in the [1 1 0] direction. Asymmetric strain relaxation in dense MD networks is a known phenomenon [19] and has been observed in $Ga_{1-x}In_xP$ grown on GaAs substrates [16]. However, the density of the MDs in sample B is found to be so small that the strain in the sample is only nominally relaxed, as evidenced by the RSM of Figs. 4(a) and (b). The hillock density $\sigma_h \approx 2000\,\mathrm{cm}^{-2}$ of sample B is similar to that of sample A.

Figs. 11(a) $\overline{2}\,\overline{2}\,0$ and (b) $\overline{1}\,5\,1$ are large-area transmission topographs of sample B. The hillock strain field images in large-area transmission topographs of sample B are practically identical to those observed in sample A in Fig. 8. In addition to the strain fields related to the hillocks the MD observed in Fig. 10 are also visible, but some of the MD images are visible in Fig. 11(a) but not in Fig. 11(b). Using the Burgers vector b criterion for disappearing contrast $g \cdot b = 0$ it follows that the Burgers vector of the MDs disappearing in Fig. 11(b) is most likely $b = a/2[1\,0\,\overline{1}]$ and the MDs are of 60° mixed $a/2\langle 1\,0\,1\rangle\{1\,1\,1\}$ type, which is a common MD type in III–V semiconductors [20,21].

All the disappearing MDs have a hillock in the middle of the dislocation line, and the contrast disappears only on the left side of the hillock in the $\overline{1}\,5\,1$ topograph of Fig. 11(a). Thus, the Burgers vectors of the MDs are not equal on the opposing sides of the hillock. Thus, the MDs either originate directly from the hillocks residing at the interface, or they are misfit segments formed by threading dislocation loop nucleation caused by the hillock formation in the upper GaInP layer, in which case the hillocks only start to grow in the later phase of the GaInP growth process. Such a MD creation process through dislocation loops having their threading segments extending and colliding into the epilayer-substrate interface and subsequently forming misfit segments at the interface is described in [19].

Matthews, Mader and Light first showed that by utilizing the mechanical equilibrium theory for minimizing the total energy of the strained epitaxial layer structure and a periodic array of MDs having a known dislocation energy, it is possible to predict the epilayer critical thickness h_c for a given MD type [22]. Matthews and Blakeslee enhanced and further established the validity of the Matthews-Blakeslee model in a series of articles [23–25]. Over the years, the mechanical equilibrium theory for calculating the critical thicknesses h_c of thin films has been generally found to reasonably agree with the experimental results [26].

The equations for critical thickness h_c derived from the equilibrium theory are of the form

$$h_c \approx \frac{b}{\Omega|f|}\left[\frac{1-\nu\cos^2\alpha}{(1+\nu)\cos\lambda}\right]\left[\ln\left(\frac{h_c}{b}\right)+\Gamma\right], \tag{1}$$

in which ν is the substrate Poisson ratio, $f = \Delta a/a$ is the lattice mismatch, b is the slip distance for the MDs i.e. the Burgers vector magnitude, $\alpha = \sphericalangle(u, b)$ is the angle between the MD line direction u and the MD Burgers vector b, and the angle $\lambda = \sphericalangle(b, u \times n)$, where n is the sample surface normal [22]. The Poisson ratio for (0 0 1) GaInP is assumed to be $\nu \approx 0.333$, and the misfit relaxation by $60°\,a/2\langle 1\,0\,1\rangle\{1\,1\,1\}$ MDs as suggested by the contrast disappearance in Fig. 11 b) corresponds to values $b = a/\sqrt{2}$ and $\cos\alpha = \cos\lambda = 1/2$. Ω and Γ are parameters related to the tension inflicted by the MD line, and they differ between authors.

Choosing $\Omega = 2\pi$, $\Gamma = 1$ and utilizing the lattice mismatches $f = \Delta a/a$ from Table 1 at RT, Eq. (1) gives a critical thickness of $h_c \approx 2.43\,\mu\mathrm{m}$ for sample A and $h_c \approx 2.22\,\mu\mathrm{m}$ for sample B, both well above the actual 1 µm $Ga_{1-x}In_xP$ epilayer thicknesses. However, using the lattice mismatches f at the growth temperature 610 °C from Table 1, the critical thickness for sample A ($h_c \approx 2.36\,\mu\mathrm{m}$) is still much larger than the actual epilayer thickness, but the critical thickness of sample B reduces to $h_c \approx 0.68\,\mu\mathrm{m}$, which is less than the actual $Ga_{1-x}In_xP$ epilayer thickness of 1 µm. Thus, the results of the Matthews-Blakeslee model with $\Omega = 2\pi$ and $\Gamma = 1$ agree rather well with the observed MD structure on the samples, provided that the effect of the growth temperature and the different linear thermal expansion coefficients α_{ltc} of the materials onto the strain are taken into account.

Fig. 12 shows the theoretical critical thickness h_c of $Ga_{1-x}In_xP$ plotted as a function of In content x according to the models suggested by Paul [27], Fischer et al. [28], Matthews–Blakeslee [22] and Matthews [29]. Because the $Ga_{1-x}In_xP$ lattice mismatch f to Ge for an In content x depends on the temperature through the linear thermal expansion coefficients α_{ltc}, the curves in Fig. 12

show the critical thickness h_c for the largest strain f within the temperature range from RT to growth temperature 610 °C. Due to the thermal strain there is no perfect $Ga_{1-x}In_xP$ lattice match to Ge, but a maximum of the critical thickness h_c. The maximum of h_c is at the In content x_{max} for which the RT and growth temperature critical thickness curves intersect.

In any case, the experimental results of this work demand that for an accurate critical thickness model, sample A having no MDs should lie below the h_c curve, and sample B having a few MDs should lie slightly above the h_c curve. Looking at Fig. 12, this only happens for the values $\Omega = 2\pi$ and $\Gamma = 1$ in Eq. (1) as suggested by Paul for single epilayers [27] and Matthews and Blakeslee for multilayer structures [23,24]. It is likely that the hillocks in the GaInP layer act as MD sources, which may affect the parameter Ω, because an individual MD can only elongate into one direction as the hillocks restrict the movement in the other direction. In the original Matthews–Blakeslee model both sides of the MD elongate, as the threading dislocations in both ends of the MD can freely slide [29]. Regardless of the exact value of the parameter Ω in Eq. (1), the Matthews–Blakeslee model appears to explain rather well the fact that there are MDs in sample B but not in sample A, provided that the linear thermal expansion coefficients α_{ltc} are taken into account.

Fig. 13 shows a 111 XRD texture map of the InP crystallites on sample B. The InP crystallites reside in the hillocks seen on the surface of sample B in the SEM micrograph of Fig. 6(b) and in the topographs of Figs. 10 and 11. The XRD texture map was recorded using InP 111 diffraction angle at $2\theta = 26.28°$. The InP diffractions can be easily distinguished from the $2\theta = 27.27°$ diffraction angle of $Ga_{0.5}In_{0.5}P$ or from the $2\theta = 28.33°$ diffraction angle of GaP, which suggests that the hillocks are made of InP with little or no Ga content. However, the small diffraction intensity levels produced by the crystallites within the hillocks made it impossible to apply more accurate HR-XRD techniques, so it could not be resolved whether there were trace amounts of Ga or not in the InP crystallites. Also, the very high intensity of the GaInP diffraction peaks S_n compared to the InP crystallite maxima causes them to appear in Fig. 13 as the XRD measurement geometry allows detecting shoulders of the high intensity GaInP peaks $\approx 1°$ off the peak center.

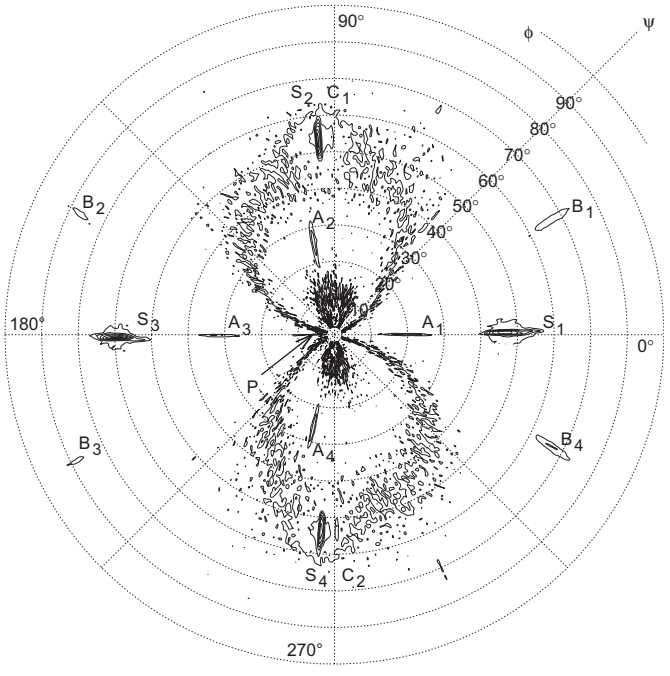

Fig. 13. XRD texture map of InP crystallites on sample B recorded using InP 111 Bragg reflection at diffraction angle $2\theta = 26.28°$ and the sample positioned at $\omega = \theta/2 = 13.14°$. The map shows the orientation of the InP crystallite ⟨111⟩ directions relative to rotation around sample surface normal (ϕ-axis), and to tilt between the diffraction plane and sample surface (ψ-axis). Intensity doubles between adjacent contours. Diffraction maxima corresponding to fourteen crystal orientations are denoted onto the figure as points S_n referring to GaInP/GaAs/Ge diffraction maxima, and points A_n, B_n and C_n referring to the observed sets of InP crystallite orientations. Also, the symmetry point, i.e. the substrate [0 0 1] position is denoted with arrow P pointing at ($\phi = 180°, \psi = 6°$).

Another interesting aspect in the XRD texture map of Fig. 13 beside the detection of diffraction maxima produced by the InP crystallites is the sharpness and high symmetry displayed by the InP diffraction maxima. The symmetry point of the ten InP and four substrate diffraction maxima is denoted with P in Fig. 13 and it is tilted 6° towards ⟨1 1 1⟩ from the surface normal, which corresponds exactly to the known 6° miscut angle of the (0 0 1) substrate. Thus, it appears that most of the observed InP crystallites on GaInP/GaAs/Ge structure grow in different lattice orientations than the substrate lattice. However, the InP crystallites nonetheless have a high degree of symmetry and well-defined crystal directions. This preservation of crystal symmetries and directions is likely the reason for the homogenous size distribution and physical form of the InP hillocks consisting of the crystallites. The high symmetry of the different InP lattice orientations suggests that each of the individual InP hillocks consists of at least 10 different crystallites having well-defined twin boundaries between each others, which would explain the observed high symmetry level.

Table 2 lists the measured real space angles between the ⟨1 1 1⟩ directions of the 12 InP crystallite orientations, as well as the angles between the high symmetry point P in Fig. 13 and the 12 InP orientations. From the angles listed in Table 2 it is indeed clear that none of the eight diffraction maxima A_n and B_n of Fig. 13 can originate from the same lattice, because the known angles 70.5° and 109.5° between different ⟨1 1 1⟩ planes of the same lattice do not fall close to any of the angles in Table 2.

It is interesting to note that the InP crystallite orientations denoted by A_n, B_n and C_n are tilted $\approx 26°$, $\approx 72°$ and $\approx 54°$ from the high symmetry point, respectively, because it indicates that the crystallites forming the hillocks grow into a system having certain rotational symmetries around the substrate lattice [0 0 1] axis. The highest-intensity diffraction maxima A_n are most likely related to the large flat facets of the InP hillocks in SEM pictures of Figs. 6(a) and (b), because the axis around which the lattice misorientation tilt occurred is of ⟨1 1 0⟩ type, which is consistent with the apparent directions of the normals of the facets in Figs. 5 and 6.

The most common twins in zincblende III–V crystals are formed by {1 1 1} planes rotating 60° around ⟨1 1 1⟩, which causes twinning angles $\theta_t = 38.94°$ and 56.25° to exist between certain ⟨1 1 1⟩ lattice directions of the two twins [30,31]. In coincidence site lattice (CSL) notation [32] these twins have a Σ3 designation. None of the measured angles between crystallite lattice orientations A_n and substrate orientations S_m in Table 2 fall close to the expected values $\theta_t = 38.94°$ or 56.25° of Σ3 boundaries. Instead, the [0 0 1] directions of the crystallite lattices corresponding to each of the diffractions A_n appear to be tilted 28° from the substrate [0 0 1] direction towards ⟨1 1 1⟩, which can be deduced from the 28° angle between diffraction maxima $\angle(A_n, S_n), n = 1, \ldots, 4$, and the relative positions of the diffraction maxima in Fig. 13. The observed 28° tilt towards ⟨1 1 1⟩ corresponds to 28° rotation about ⟨1 1 0⟩ axis, which is fairly close to the well-known Σ19 CSL tilt misorientation of 26.53° about a ⟨1 1 0⟩ axis [33]. Because the observed rotation axis ⟨1 1 0⟩ is exactly the same as would be expected for Σ19 twins grown onto the substrate, and because the 1.5° difference

Table 2
Angles in real space between ⟨1 1 1⟩ crystal directions for different orientations in InP crystallites were determined from Fig. 13.

Crystallite orientation	C_2 (deg)	C_1 (deg)	B_4 (deg)	B_3 (deg)	B_2 (deg)	B_1 (deg)	A_4 (deg)	A_3 (deg)	A_2 (deg)	A_1 (deg)	S_4 (deg)	S_3 (deg)	S_2 (deg)	S_1 (deg)
S_1	66	66	30	120	119	31	58	80	57	28	70	107	69	
S_2	107	4	99	99	58	59	79	58	28	58	107	70		
S_3	73	73	121	29	29	121	57	28	58	79	69			
S_4	4	108	59	58	98	100	28	57	79	58				
A_1	56	56	50	95	94	51	36	51	35					
A_2	79	29	85	85	62	63	51	36						
A_3	60	60	96	49	48	97	36							
A_4	28	80	63	62	83	86								
B_1	97	55	50	145	116									
B_2	102	61	143	50										
B_3	62	102	117											
B_4	55	97												
C_1	108													
Symmetry center P	54	54	72	72	71	73	26	27	25	25	54	54	54	53

The 12 orientation maximas are labeled in Fig. 13. Angles between the symmetry center P in Fig. 13 and the closest ⟨1 1 1⟩ direction of the InP orientations are also given.

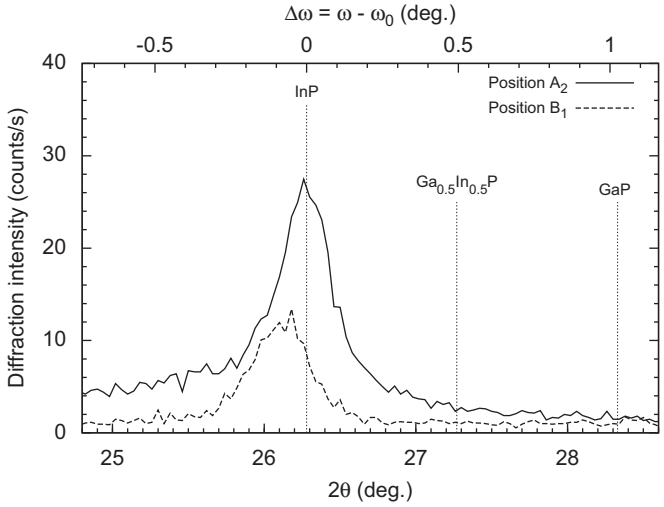

Fig. 14. $2\theta/\omega$1 1 1 XRD curves of InP crystallites on sample B recorded using ϕ,ψ-positions A_2 and B_1 from Fig. 13. $\Delta\omega=\omega-\omega_0$, in which ω is the angle between the sample surface and the incident X-ray beam, and $\omega_0=13.07^\circ$ for position A_2 and $\omega_0=13.14^\circ$ for position B_1. Vertical lines indicate lattice plane spacings corresponding to 1 1 1 diffractions of InP, $Ga_{0.5}In_{0.5}P$ and GaP.

between the measured and expected twinning angles is within the measurement uncertainty, it is likely that the diffraction maxima A_n correspond to crystallites which are connected to the epilayer lattice through Σ19 twin boundaries. Moreover, because the interface between the InP hillock lattice and the GaInP layer lattice is necessarily a heterointerface, the difference in the lattice constants likely causes additional tilting within the twinned interfaces. Thus, an individual hillock is probably connected to the epilayer lattice through four distinct Σ19 twin boundaries of four distinct crystallites forming the base of the hillock. The other observed diffraction maxima in Fig. 13 are believed to be related to a more complex structure of twinned crystallites necessary to connect the four Σ19 twins together.

Fig. 14 shows two $2\theta/\omega$ XRD curves recorded from the crystallites on sample B. The $2\theta/\omega$ diffraction curves of the crystallite orientations A_2 and B_1 of Fig. 13 can be used for the evaluation of lattice spacing d of the crystallites. The expected diffraction maxima positions of InP, $Ga_{0.5}In_{0.5}P$ and GaP single crystals are marked onto the figure. It is clear that within the measuring accuracy the crystallites mainly consist of InP. The measurement accuracy is limited by the 0.2° acceptance angle of the collimator in front of the X-ray detector. Due to the wide acceptance angle of the XRD geometry used, the accuracy of the measurement is not comparable to the HR-XRD measurements, and a small Ga content in the crystallites can not be ruled out. Also, the center of the smaller B_1 peak is on the left side of the InP lattice constant, which is believed to be caused by small tensile strain affecting the part of the InP lattice having an orientation corresponding to diffraction maxima B_n in Fig. 13.

Notwithstanding the measurement uncertainty, the XRD curves of Fig. 14 further suggest that the hillocks are made of InP. However, it should be noted that there may well exist less ordered parts of the hillocks not visible in the XRD spectra and containing materials other than InP. In the GaInP/GaAs structure studied in [5] similar hillocks are observed to consist of an In-rich base region and of Ga-rich particulates. However, due to the relatively strong XRD intensity recorded from the InP crystallites in this work, it is safe to conclude that significant parts of the hillocks are made of rigorously ordered InP crystallites, which are connected to each other by twinned grain boundaries.

4. Conclusions

The SR-XRT images of the GaInP layers grown on the GaAs/Ge substrates revealed the existence of MDs in the epitaxial GaInP layer of sample B, despite the sample having a relatively small lattice mismatch to Ge at RT. However, the SR-XRT images of sample A proved that relatively thick (1 μm) MD-free GaInP epilayers can be grown on GaAs/Ge, if the In content x in the $Ga_{1-x}In_xP$ epilayer was selected so that the absolute value of the lattice mismatch between $Ga_{1-x}In_xP$ and Ge in the temperature range from RT to the growth temperature of 610 °C was minimized. The results were compared to theoretical predictions about critical thickness h_c, and a good agreement was found provided that the thermal expansion at growth temperature was taken into account.

It appears that the 240-nm-thick GaAs buffer layer does not play a significant role in the MD formation due to its relatively small thickness. Notwithstanding this, its role as a straightforward way to acquire high-quality polar III–V surfaces for Ge substrates makes it important in the effort to grow high-quality GaInP on Ge. The GaAs/Ge substrates are believed to be a feasible basis for epitaxial GaInP devices of the future.

InP hillocks similar in their appearance to those typical for GaInP/GaAs layers [4–7] were also found in the GaInP layers grown on GaAs/Ge substrates. The InP hillocks had a surface density of $\approx 2000\,cm^{-2}$, and they were observed to be very

homogenous in their faceted form, crystallite orientations and size ($\approx 6 \times 12\,\mu m^2$). The hillocks were found to consist of a rigorous system of twinned crystallites connected to each other. Also, the strain fields produced by the InP hillocks into the GaInP lattice were very homogenous, suggesting a strictly deterministic process producing the hillocks during the MOVPE growth. Although the faceted InP hillocks are unintentional, their homogeneity and the fact that they are made of a different material in different crystal orientation than the surrounding lattice might turn out advantageous if utilized as a part of a self-organized growth process.

Acknowledgments

The authors thank Dr. Carsten Paulmann for providing assistance at HASYLAB beamline F1 Topography. The authors also acknowledge financial support by the European Community - Research Infrastructure Action under the FP6 "Structuring the European Research Area" Program (through the Integrated Infrastructure Initiative "Integrating Activity on Synchrotron and Free Electron Laser Science") under the HASYLAB project DESY-D-II-20060222 EC.

References

[1] T. Takamoto, M. Kaneiwa, M. Imaizumi, M. Yamaguchi, InGaP/GaAs-based multijunction solar cells, Prog. Photovoltaics: Res. Appl. 13 (2005) 495–511.
[2] L. Knuuttila, A. Lankinen, J. Likonen, H. Lipsanen, X. Lu, P. McNally, J. Riikonen, T. Tuomi, Low temperature growth GaAs on ge, Jpn. J. Appl. Phys 44 (2005) 7777–7784.
[3] A. Lankinen, L. Knuuttila, T. Tuomi, P. Kostamo, A. Säynätjoki, J. Riikonen, H. Lipsanen, P.J. McNally, X. Lu, H. Sipilä, S. Vaijärvi, D. Lumb, Synchrotron X-ray topography study of defects in epitaxial GaAs on high-quality Ge, Nucl. Instr. Meth. Phys. A 563 (2006) 62–65.
[4] H. Hamada, M. Shono, S. Honda, R. Hiroyama, K. Yodoshi, T. Yamaguchi, AlGaInP visible laser diodes grown on misoriented substrates, IEEE J. Quant. Electron. 27 (1991) 1483–1490.
[5] M.J. Matragrano, V. Krishnamoorthy, D.G. Ast, J.R. Shealy, Characterization and elimination of surface defects in GaInP, J. Cryst. Growth 142 (1994) 275–283.
[6] S. Hasenöhrl, R. Kúdela, J. Novák, T.O. Tuomi, L. Knuuttila, Anisotropic faceted structure in ordered strained InGaP, Mat. Sci. Eng. B 88 (2002) 134–138.
[7] J. Novák, S. Hasenöhrl, R. Kúdela, M. Kučera, Growth and characterisation of InGaP layers with composition close to crossover from direct to indirect band gap, J. Cryst. Growth 275 (2005) e1281–e1286.
[8] T. Tuomi, K. Naukkarinen, P. Rabe, Use of synchrotron radiation in X-ray diffraction topography, Phys. Stat. Sol. (a) 25 (1974) 93–106.
[9] T. Tuomi, Synchrotron X-ray topography of electronic materials, J. Synchrotron Radiation 9 (2002) 174–178.
[10] G.A. Slack, S.F. Bartram, Thermal expansion of some diamond like crystals, J. Appl. Phys. 46 (1975) 89.
[11] I. Kudman, R.J. Paff, Thermal expansion of InGaP alloys, J. Appl. Phys. 43 (1972) 3760.
[12] J.F.C. Baker, M. Hart, An absolute measurement of the lattice parameter of germanium using multiple-beam X-ray diffractometry, Acta Crystallogr. 31a (1975) 364–367.
[13] S. Kishino, Improved techniques of lattice parameter measurements using two X-ray beams, Adv. X-Ray Anal. 16 (1973) 367.
[14] G. Giesecke, H. Pfister, Präzisionsbestimmung der gitterkonstanten von aiiibv-verbindungen, Acta Crystallogr. 11 (1958) 369–371.
[15] H. Nagai, Structure of vapor-deposited GaInAs crystals, J. Appl. Phys. 45 (1974) 3789–3794.
[16] M.J. Matragrano, D.G. Ast, J.R. Shealy, V. Krishnamoorthy, Anisotropic strain relaxation of GaInP epitaxial layers in compression and tension, J. Appl. Phys. 79 (1996) 8371–8378.
[17] M.K. Lee, R.H. Horng, L.C. Haung, MOCVD growth of GaInP ordered alloy by phosphine modulation, in: Metalorganic Vapor Phase Epitaxy, Sixth International Conference, 1992, pp. 258–259.
[18] B.K. Tanner, Xray Diffraction Topography, Pergamon Press, 1976, pp. 71–86.
[19] A. Capano, L. Hart, D.K. Bowen, D. Gordon-Smith, C.R. Thomas, C.J. Gibbings, M.A.G. Halliwell, L.W. Hobbs, Strain relaxation in $Si_{1-x}Ge_x$ layers on Si (0 0 1), J. Cryst. Growth 116 (1992) 260–270.
[20] D.J. Eaglesham, D.M. Maher, E.P. Kvam, J.C. Bean, C.J. Humphreys, New source of dislocations in Ge_xSi_{1-x}/Si(1 0 0) strained epitaxial layers, Phys. Rev. Lett. 62 (1989) 187–190.
[21] Y.H. Lo, New approach to grow pseudomorphic structures over the critical thickness, Appl. Phys. Lett. 59 (1991) 2311–2313.
[22] J.W. Matthews, S. Mader, T.B. Light, Accommodation of misfit across the interface between crystals of semiconducting elements or compounds, J. Appl. Phys. 41 (1970) 3800–3804.
[23] J.W. Matthews, A.E. Blakeslee, Defects in epitaxial multilayers—I. misfit dislocations, J. Cryst. Growth 27 (1974) 118–125.
[24] J.W. Matthews, A.E. Blakeslee, Defects in epitaxial multilayers—II dislocation pile-ups, threading dislocations, slip lines and cracks, J. Cryst. Growth 29 (1975) 273–280.
[25] J.W. Matthews, A.E. Blakeslee, Defects in epitaxial multilayers—III. preparation of almost perfect multilayers, J. Cryst. Growth 32 (1976) 265–273.
[26] J.P. Hirth, Some current topics in dislocation theory, Acta Mater. 48 (2000) 126–133.
[27] D.J. Paul, Si/SiGe heterostructures: from material and physics to devices and circuits, Semicond. Sci. Technol. 19 (2004) R75–R108.
[28] A. Fischer, H. Kühne, H. Richter, New approach in equilibrium theory for strained layer relaxation, Phys. Rev. Lett. 73 (1994) 2712–2715.
[29] J.W. Matthews, Accommodation of misfit across the interface between crystals of semiconducting elements or compounds, J. Vac. Sci. Technol. 12 (1975) 126–133.
[30] W.T. Read, W. Shockley, Dislocation models of crystal grain boundaries, Phys. Rev. 78 (1950) 275–289.
[31] B.A. Korgel, Twins cause kinks, Nat. Mater. 5 (2006) 521–522.
[32] V. Randle, The coincidence site lattice and the sigma enigma, Mat. Charact. 47 (2001) 411–416.
[33] H. Kung, P.G. Sanders, J.R. Weertman, Transmission electron microscopy characterization of nanocrystalline copper, in: Y.-W. Chung, D.C. Dunand, P.K. Liaw, G.B. Olson (Eds.), Advanced Materials for the 21st Century, 1999, pp. 455–463.